Intelligent Computing
A SCIENCE PARTNER JOURNAL

RESEARCH ARTICLE

Challenging Point Scanning across Electron Microscopy and Optical Imaging using Computational Imaging

Akhil Kallepalli[1*†], Lorenzo Viani[2,3†], Daan Stellinga[4†], Enzo Rotunno[3*†], Richard Bowman[1], Graham M. Gibson[1], Ming-Jie Sun[5], Paolo Rosi[2,3], Stefano Frabboni[2,3], Roberto Balboni[6], Andrea Migliori[6], Vincenzo Grillo[3], and Miles J. Padgett[1]

[1]School of Physics and Astronomy, University of Glasgow, Glasgow, G12 8QQ, UK. [2]Department of Physics, IT, and Mathematics, University of Modena and Reggio Emilia, Via Campi 213/A, 41125 Modena, MO, Italy. [3]CNR-NANO, Via G. Campi 213/A, 41125 Modena, Italy. [4]Faculty of Science and Technology, University of Twente, Enschede, The Netherlands. [5]School of Instrumentation and Optoelectronic Engineering, Beihang University, Beijing 100191, China. [6]CNR-IMM, Via Gobetti 101, 40129 Bologna, Italy.

*Author correspondence to: akhil.kallepalli@glasgow.ac.uk
†These authors contributed equally to this work.

Solving challenges of enhanced imaging (resolution or speed) is a continuously changing frontier of research. Within this sphere, ghost imaging (and the closely related single-pixel imaging) has evolved as an alternative to focal plane detector arrays owing to advances in detectors and/or modulation devices. The interest in these techniques is due to their robustness to varied sets of patterns and applicability to a broad range of wavelengths and compatibility with compressive sensing. To achieve a better control of illumination strategies, modulators of many kinds have long been available in the optical regime. However, analogous technology to control of phase and amplitude of electron beams does not exist. We approach this electron microscopy challenge from an optics perspective, with a novel approach to imaging with non-orthogonal pattern sets using ghost imaging. Assessed first in the optical regime and subsequently in electron microscopy, we present a methodology that is applicable at different spectral regions and robust to non-orthogonality. The distributed illumination pattern sets also result in a reduced peak intensity, thereby potentially reducing damage of samples during imaging. This imaging approach is potentially translatable beyond both regimes explored here, as a single-element detector system.

Citation: Kallepalli A, Viani L, Stellinga D, Rotunno E, Bowman R, Gibson GM, Sun MJ, Rosi P, Frabboni S, Balboni R, Migliori A, Grillo V, Padgett MJ. Challenging Point Scanning across Electron Microscopy and Optical Imaging using Computational Imaging. *Intell. Comput.* 2022;2022:Article 0001. https://doi.org/10.34133/icomputing.0001

Submitted 25 July 2022
Accepted 15 October 2022
Published 21 December 2022

Copyright © 2022 Akhil Kallepalli et al. Exclusive licensee Zhejiang Lab. No claim to original U.S. Government Works. Distributed under a Creative Commons Attribution License 4.0 (CC BY 4.0).

Downloaded from https://spj.science.org on April 24, 2023

Introduction

At a fundamental level, the principles governing optical and electron beams are identical. Electron microscopy achieves resolutions (40 pm for transmission electron microscopy (TEM) and scanning transmission electron microscopy (STEM) and up to 20 pm using ptychography [1]) below atomic distances and is capable of achieving a greater depth of field and magnification of up to 250 times the limit of light microscopes. However, the creation of new elements that could harness the electrostatic and magnetic fields in an electron microscope is technologically challenging. It is, therefore, no surprise that electron microscopy relies on elementary waveform-like plane waves or uses very tiny convergent probes. A huge technological effort was achieved in controlling the aberrations in the beam, but there remains a need to achieve additional complex phase and amplitude control in these microscopes. Our study here explores the application of a novel imaging algorithm that is robust to non-orthogonal illumination strategies across 2 electromagnetic regions—optical wavelengths and electron beams. We present an approach that is tested first in the optical regime with spatial light modulators (SLMs) using non-orthogonal pattern sets. Subsequently, the algorithm is used to reconstruct an imaging target in a transmission electron microscope with a beam modulation device.

Modulation in optics using wavelengths of light is technologically substantially ahead. The phase and amplitude of light can be modulated using SLMs. These modulators use deformable mirrors, digitally controlled micromirrors, or liquid crystals, and the choice of the device depends on the application. These devices allow pixel-wise control of the waveform. These devices are not available for electron microscopists, and the best alternatives have comparatively limited functionality [2].

Years of research and innovation have shown that although structured electron probes have been realized, these are yet to challenge the status quo of real imaging of materials and nanostructures. In this work, we use novel algorithms and beam shaping to demonstrate that robust control is possible in

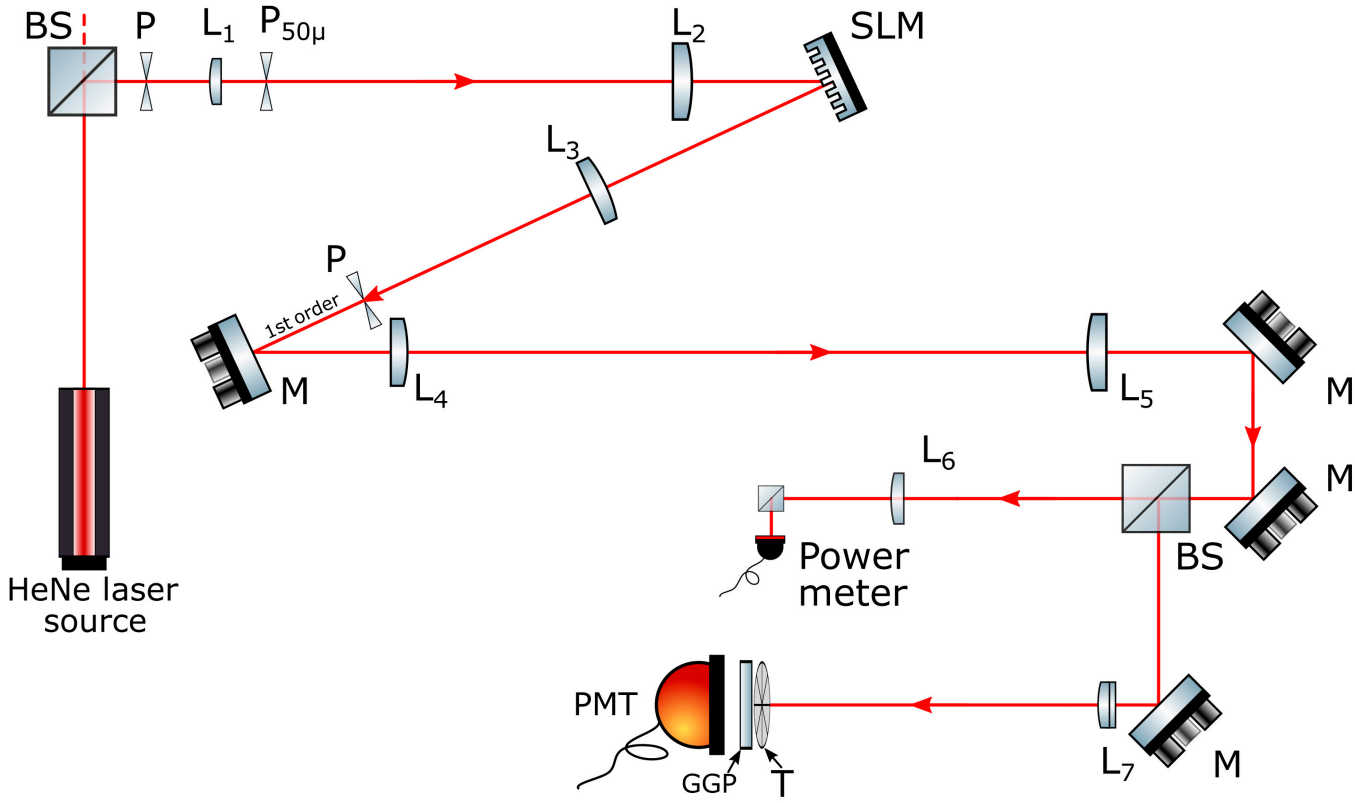

Fig. 1. Light from a HeNe laser at 633 nm is polarized by a polarizing beam splitter (PBS), then spatially filtered and expanded to fill the aperture of an SLM using an aperture (P), a 50-mm focal length lens (L_1), precision pinhole ($P_{50\mu}$), and 400-mm lens (L_2). The SLM displays a superposition of the 6-needle phase masks and a carrier diffraction grating. The SLM is optimized to project the majority of the modulated light into the first diffraction order, which is selected using a 250-mm lens (L_3) and aperture (P) placed in the Fourier plane of the SLM. This light is propagated into the far field through a combination of lenses (250-mm focal length lens (L_4) and 400-mm focal length lens (L_5)). The beam is propagated into 2 separate arms using a beam splitter (BS). One arm uses a power meter to measure the laser power and the second arm consists of the target (T) in front of a ground glass plate (GGP). The photomultiplier tube (PMT) measures the transmitted light after interaction with the target. Author figure was adopted from Kallepalli et al. [30].

electron microscopy with the ability to project and image using complicated far-field patterns. With significant contributions to both optical and electron microscopy regimes, a truly interdisciplinary solution is achieved and presented in this article.

Scanning transmission electron microscopes achieve high-resolution imaging by point-scanning the sample with a focused beam of electrons. The interaction of the electron beam with the sample and the resulting measurement is used to form an image. Point scanning (also known as raster scanning) is a simple approach to creating an image in the absence of complicated detector arrays. An alternative approach that has been pioneered in the optical regime has been measuring the transmission of the sample when illuminated with more complicated spatial patterns. This approach, often referred to as computational ghost imaging (CGI), inverts knowledge of the projected patterns and their measured transmission to reconstruct the image. While this method has been used for a megaelectron volt (MeV) electron beam by modulating directly the cathode photoemission [3] and, more recently, theoretically based on electron light interaction [4,5], it has never been demonstrated in a TEM using coherent beam shaping. The coherence is key, as this allows potentially achieving atomic resolution imaging in the future.

The spatial structuring of optical beams has been extended to matter waves, primarily electrons. This structuring of electron beams paved the way for the production of vortex electron beams [6–8], self-accelerating beams [9], non-diffracting beams [10–12], and orbital angular momentum analyzers [13,14]. In the case of electron beams, an arbitrary way of spatially programming flexibly a beam is problematic, and existing methods for the dynamic shaping of electron beams are limited.

Since the time-independent wave equation for the light and electrons are analogous [15], components such as lenses for electron beams are defined with a similar nomenclature as for light. Although single-element detector-based imaging has previously been introduced for specialized electron imaging systems [16,17], the barrier to more general use is the absence of SLM-like technologies. Holographic plates [15,18] laid the foundation for applications related to the shaping of electron beams. However, these are passive elements and cannot be dynamically addressed similar to optical SLMs. A recent development has been the introduction of active optical elements or programmable phase plates [2]. These are based on simple electrostatic elements to be positioned along the beam path. Two technological solutions are available. The research group led by Verbeeck [2] has been developing devices based on Einzel lenses. These lenses work similar to the individual pixels of an optical SLM, but the number of addressable points are few in comparison to the optical devices [2]. An additional challenge for these lenses arises from the difficulty to bias and drive many connections from outside the microscope column, which necessarily limits the useful fill fraction of such a pixel-based approach.

Downloaded from https://spj.science.org on April 24, 2023

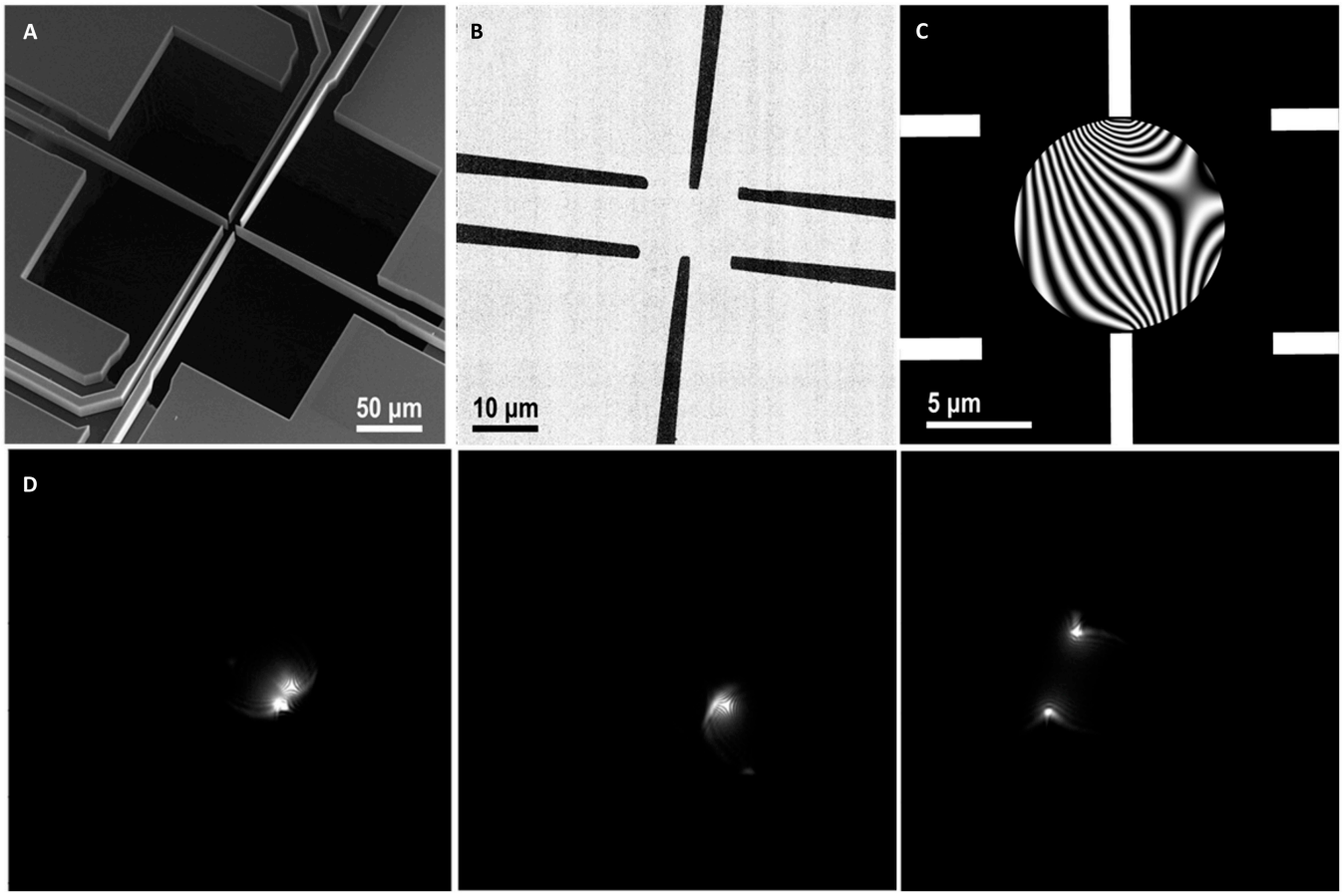

Fig. 2. The pattern sets are inspired from needle arrangements used to modulate electron beams. Scanning electron microscopy images (A) and (B) illustrate the 6-needle device and its active region. The active region is limited by a 10-μm-diameter aperture, and a resulting simulation of a typical phase profile produced by these needles is shown in (C). The white bars in (C) show the positions of the needles. (D) Three TEM experimental images of the intensity distribution in the far field produced by the device. Similar intensity profiles are generated in the optical experiment (Fig. 1) using phase modulation.

As an alternative, using separated electrodes to define specific phase landscapes across a wider area have been explored. This electrode-based approach has the benefit that the beam itself only interacts with the electric field created rather than the modulator components themselves, avoiding the main problems of the other approach. However, the solution is defined spatially where the phases ϕ are limited by the harmonic condition $\nabla^2\phi = 0$ except on the electrodes [19]. In other words, the potential for high-resolution phase modulation remains restricted.

The most trivial electrode in use is a simple metallic needle [20]. The definition of the electrostatic field around a charged microtip has been studied in detail [21,22], wherein charge applied to these needles induces a phase shift to the electron beam. Interestingly, the phase shift generated by a metallic needle was used to implement an orbital angular momentum sorter [14,23,24]. More importantly, multiple metallic needles have been demonstrated the ability to produce complex tunable caustic phenomena in the far field [25]. This current work uses an arrangement of 6 such needles.

The flexibility in the image formation permits optimization of different aspects of imaging. For instance, it is possible to decrease the dose in the imaging with a combination of the proposed method and compressive sensing strategies [26–28], to increase the resolution by including superoscillatory features in the illuminating beam [29] and/or control the dose rate for each area and increase the resolution by including the aberrations limiting the resolution within the mechanism of caustic generation (as discussed in Appendix S2) [4].

Methods and Results

Ghost imaging algorithm

The advantages of the computational ghost imaging are 2-fold. First, single-element detectors usually have better characteristics. For light, an extended range of operating wavelengths and a larger quantum efficiency for electrons (although with advancements in technology, this advantage is strongly reducing). Second, the flexibility of the illuminating patterns make them potentially more suitable for optimization through compressed sensing strategies wherein an image is reconstructed using a subset of the pattern set and achieving a comparable resolution [31–33]. This ability to image with fewer measurements increases the frame rate and/or reduces the exposure of delicate samples to potentially damaging illumination. Specifically in the case of electrons, the use of CGI permits modification/optimization of the dose rate and dwell time at specific regions of the sample. Recent studies suggest that tuning these parameters is key to allow for partial healing of damages [3,34] or reduction in damage [4]. A discussion about these effects has been included in Appendix S1. It is worth mentioning that the

Downloaded from https://spj.science.org on April 24, 2023

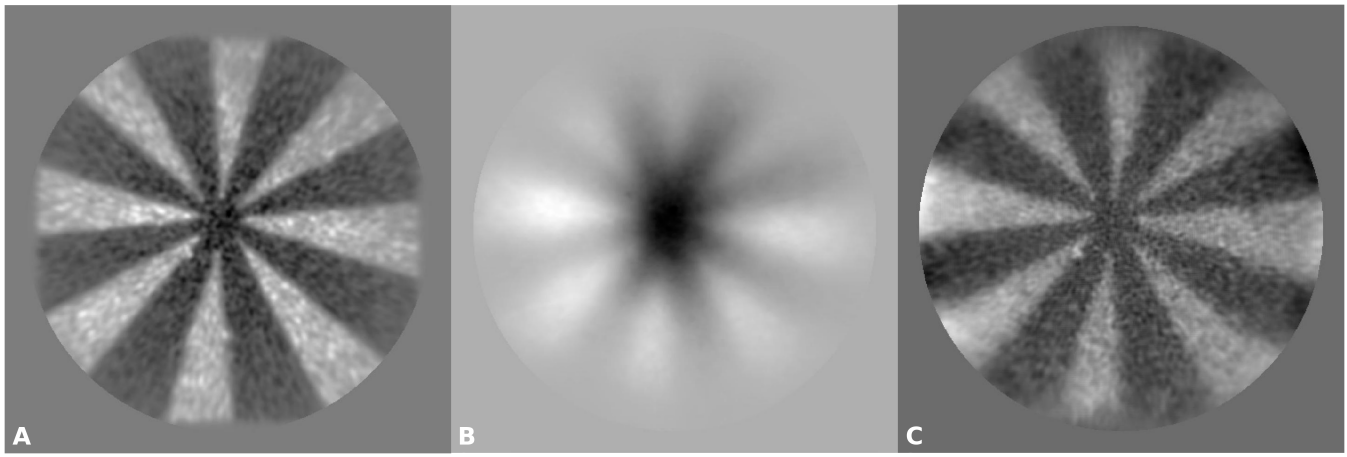

Fig. 3. Our approach illustrates the viability of using TEM-inspired phase masks for image reconstruction using a new approach to ghost imaging known as orthogonalized ghost imaging (OGI). This approach is ideal for cases such as 6-needle phase mask sets, where the pattern set is not orthogonal. The comparison shows (A) randomized point scan (raster scan) using traditional ghost imaging (TGI), (B) 6-needle phase masks using TGI, and (C) 6-needle phase masks using the proposed OGI technique. In each case, the construction was done using a set of 50,000 patterns, and the reconstructed images are of 512-pixel × 512-pixel resolution. The binary, laser-cut amplitude target consists of 8 spokes and is of a physical size of 10 mm.

coherent aberration that is currently one of the limiting factor for electron microscopy resolution could be included in the CGI scheme without a need to correct them, allowing therefore a new scheme for increased resolution. Using these computational ghost imaging techniques, systems have been developed that include imaging at terahertz wavelengths [35], time-of-flight imaging [36,37], and fluorescence lifetime imaging [38].

The choice of mask patterns is key to the performance of the single-element detector-based systems, as it defines the resolving capability of the system and the applicability of the reconstruction algorithm. The field of ghost imaging has seen an evolution in experimental setups and algorithms [3,39,40]. Although the vast majority of computational ghost imaging and the related work on single-pixel cameras use a spatial modulator positioned in the image plane of the object, the original work by Shapiro [41] recognized that this need not be the case. Rather, given any specific modulation, the resulting form of the light field in the plane of the object could be calculated using numerical beam propagation techniques enabling both lens-free and far-field implementations [28]. Here lies the governing principle of this effective translation of the novel orthogonalized ghost imaging (OGI) in optical methods to imaging in TEM.

Ghost imaging techniques use the knowledge of the patterns and the measurements from the detector to recover an image. This problem, mathematically, can be described in a simple matrix form:

$$A\vec{x} = \vec{b}, \tag{1}$$

where A is a matrix containing the patterns $\overrightarrow{P_i}^{\mathsf{T}}$ as rows, $\vec{x}$ is the (vectorized) scene, and $\vec{b}$ is the set of measurements b_i. The methods used to retrieve $\vec{x}$, and thereby, an image fall broadly into 2 categories: offline or online methods [42]. Offline approaches infer the image from the final, complete set of patterns and corresponding measurements. The majority of well-known methods for solving linear systems fall in this category, such as the matrix (pseudo-)inversion, Newton's method, gradient descent, etc. Conversely, online approaches update a "best guess" of the image with every new measurement and pattern. The most common online algorithm used in ghost imaging involves a straightforward weighted sum of the patterns, where the weights are adjusted on the basis of a statistical interpretation of the measurements:

$$\vec{g}_i = \vec{g}_{i-1} + \left(b_i - \langle b\rangle_i\right)\vec{p}_i. \tag{2}$$

Here, $\vec{g}_i$ is the best estimate after i patterns, $\langle b\rangle_i$ indicates the mean detector value up to the current pattern, and $\vec{g}_0 = \vec{0}$. This algorithm, which we will refer to as traditional ghost imaging (TGI), has been extensively explored with different setups [43,44].

In a standard ghost imaging system, the number of illumination patterns required is typically equal to the number of pixels in the image. This quickly makes the matrix A from Eq. 1 very large, leading to high memory requirements and long computation times for offline methods. The primary advantage of online reconstruction algorithms lies in the low computational overhead and robustness to undersampling. Online methods only need to store the current best guess of $\vec{x}$ and the current pattern, can run in parallel with the measurement, and only ever operate on vectors of limited size. Moreover, OGI is, by its very nature, impervious to problems with undersampling and can show approximations to the correct image with comparatively only a handful of measurements.

Both classes of reconstruction methods work significantly better when used with orthogonal pattern sets such as Hadamard matrices [45–47], where each mask probes a subset of spatial frequencies. For offline methods, this is equivalent to ensuring full row rank, which increases the stability of the matrix inversion results. For TGI, it ensures that each pattern's spatial frequencies are counted democratically in the mean correction term. Either way, in the absence of noise, the result approaches the true image when the number of orthogonal patterns equals the number of pixels.

If the mask patterns are implemented using a pixelated SLM, then specifying their design to be orthogonal is straightforward (e.g., Hadamard or similar). If, however, the patterns

Downloaded from https://spj.science.org on April 24, 2023

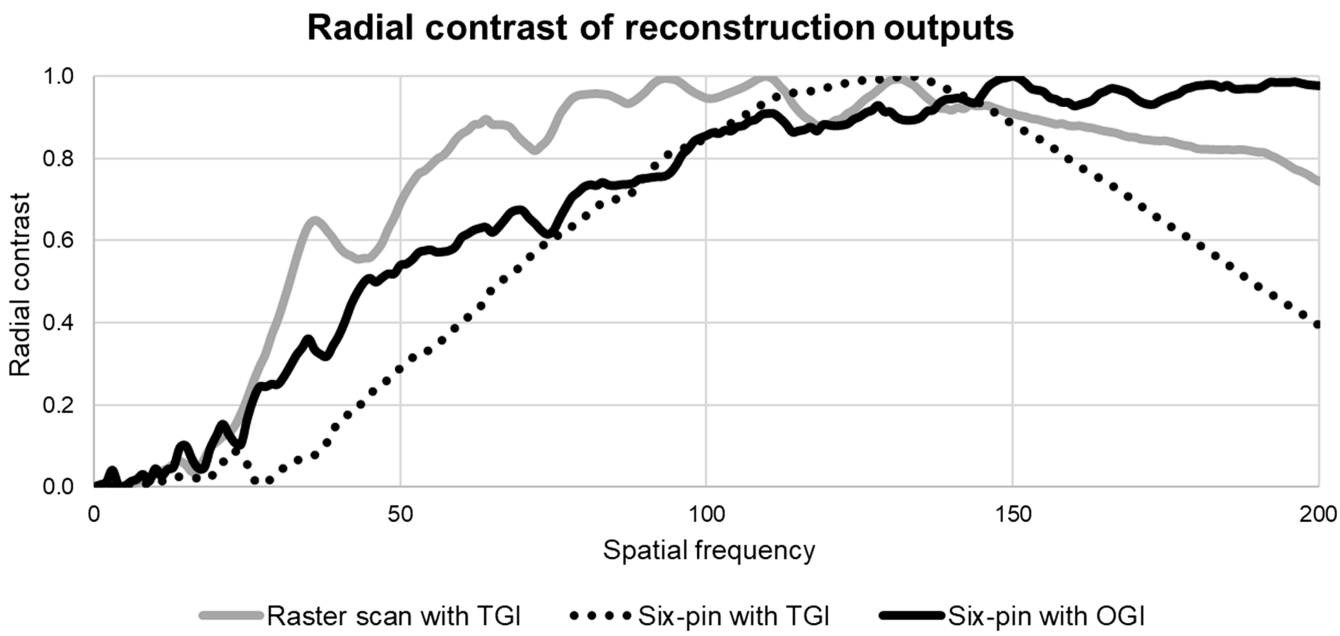

Fig. 4. Radial contrast functions associated with the images shown in Fig. 3, quantifying the resulting reconstructions using OGI–6 needles, TGI–6 needles, and TGI–raster scans, each using 50,000 patterns. The 6-needle patterns are non-orthogonal by nature.

are produced in other ways, e.g., using natural scattering or with the highly limited modulators such as those available in TEM, then orthogonality between the patterns can no longer be enforced and the standard reconstruction algorithms typically no longer converge to an accurate image. The TGI algorithm in particular will overemphasize the overlapping parts of the patterns. To resolve this issue, we present an alternative approach that is computationally efficient and makes optimal use of patterns regardless of their orthogonality. This alternative method, which we coined as OGI, takes inspiration from the Kaczmarz algorithm for solving linear systems [48–52].

OGI essentially takes the projection of each new pattern onto the current best pattern estimate as an extra correction to the mean detector value used in TGI:

$$\vec{g}_i = \vec{g}_{i-1} + \left[\left(b_i - \langle b\rangle_i\right) - \left(c_i - \langle c\rangle_i\right)\right]\vec{p}_i, \qquad (3)$$

where $c_i = \vec{p}_i \cdot \vec{g}_{i-1}$ is the predicted signal under the assumption that the previous best estimate is the correct reconstruction. This has the effect of mitigating double counting stemming from non-orthogonality and emphasizing only the new information in the measurement. Note that care needs to be taken to ensure that the measured and predicted values are correctly scaled to each other such that the reconstructed image approaches the true image. Mathematically, this is expressed such that the quantity $[(b_i - \langle b\rangle_i) - (c_i - \langle c\rangle_i)]$ tends to 0. The approach we adopt to ensure this scaling is to renormalize the signals at each iteration such that $\langle c\rangle = \langle b\rangle$ and (SDs) $\sigma_c = \sigma_b$.

In application, the approach of improving the reconstruction iteratively can be considered a "self-learning" method as the final reconstruction improves with each iteration. The robustness of OGI to non-orthogonal patterns, in addition to all the advantages mentioned above, enhances the imaging capabilities at any wavelength. Since CGI is a largely applied and flexible imaging, future development can be used to further optimize the imaging and, for example, reduce the dose and the number of necessary pattern with compressed sensing, an accurate use of any prior information in the choice of the pattern and reconstruction using regression or other optimization tools [53]. However, this approach has the advantage of being quickly implemented and converges rapidly to an intelligible solution. This is an advantage in near real-time applications as an alternative to raster scanning.

Optical verification of ghost imaging with non-orthogonal patterns

To confirm the algorithm's performance and its application, an optical experiment analogous to the TEM system was set up to test the illumination strategy and OGI algorithm's robustness to non-orthogonality. This optical experiment (Fig. 1) modulates the phase of a laser beam to produce complex point spread functions in the far field of the modulator (SLM). The modulation itself is inspired from the charged microtips approach designed by Matteucci et al. [21] as used in the electron microscope. In the TEM arrangement, random voltages are applied to the needles (as shown in Fig. 2A to C) to create a spatially structured phase change in the transmitted electron beam. This leads to complicated, spatially structured, point spread functions in the far field (Fig. 2D) that illuminate the sample. In the optical analogy, the equivalent phase change is induced using a liquid crystal SLM. The experiments were carried out in the LabView environment, using an Intel Core i9-10940X CPU with 128 GB of memory. A standard helium neon (HeNe) laser source operating at 633 nm was used to illuminate the XY series SLM (Meadowlark Optics) capable of phase and amplitude modulation at a 512-pixel × 512-pixel resolution. The intensity measurement is done using the PMM02 photomultiplier tube (PMT) module (Thorlabs Inc.).

The 6-needle approach to ghost imaging is demonstrated optically using the set up shown in Fig. 1. The expanded output beam from a HeNe laser is shaped using randomly switched 6 needles that generate phase masks. These phase masks are

Downloaded from https://spj.science.org on April 24, 2023

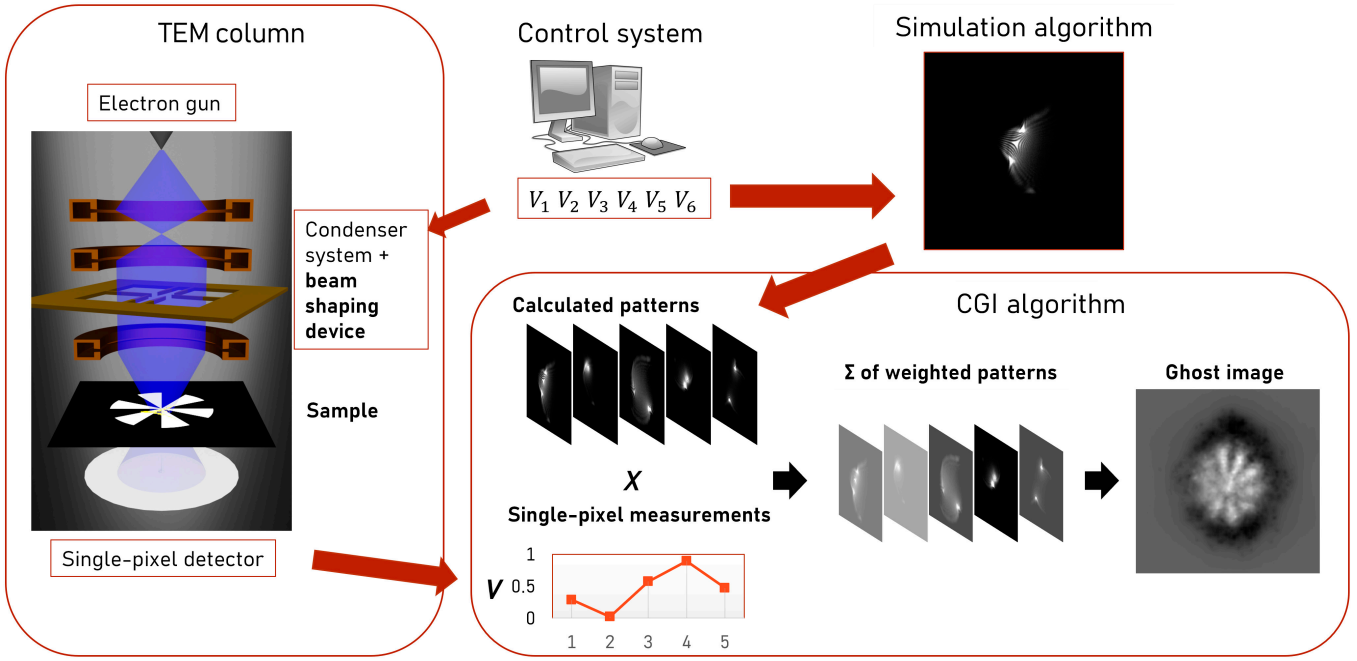

Fig. 5. A TEM sample holder carrying our needle-based beam-shaping device is inserted in the column at the condenser system level. Dedicated electronics are used to randomly select 6 random biases and apply them to the needles. The electron beam crosses the potential distribution and is imaged on the sample. Then, the total transmitted intensity is acquired by a single-pixel detector, whose output value is acquired by the electronics and recorded together with the 6 biases. After that, the patterns used for the measurement are calculated starting from the 6 biases. Finally, the combination of the single-pixel measurements and the calculated patterns through the CGI algorithm yields the ghost image of the sample.

displayed on the SLM, structuring the laser beam and propagating complex intensity patterns into the far field. The SLM operates in a diffractive mode, and therefore, the phase masks are combined with a carrier phase grating to diffract the desired pattern to the first order that is selected by a pinhole in the Fourier plane. The chosen order is then propagated through the lens system and into 2 paths: (a) laser power meter to monitor the laser power for any variations and (b) ghost imaging system (PMT). The PMT is positioned to collect the light after transmission by the object. These measurements and the knowledge of phase masks allow image reconstruction using the TGI and OGI algorithms.

We benchmark the performance of this approach against point scanning. Point scanning is done by displaying a series of linear phase gratings on the SLM to produce a scanning spot in the far field. Subsequently, the 6-needle approach to modulate the light is used and images are reconstructed. The results, shown in Fig. 3, give a visual representation of the TGI and OGI algorithm performance compared to that of a raster scan, when imaging an object that is 10-mm wide (diameter). The algorithm reconstructs a 512-pixel × 512-pixel image with 50,000 patterns (effectively, undersampled). This illustrates both the value of ghost imaging for reconstructing images through undersampling and the robustness of the algorithms. For randomized point scanning, each projection of a high-intensity spot is treated as a pattern, and the algorithms are applied for reconstruction. Furthermore, although Fig. 2D illustrates that the point spread function in the far field are localized, i.e., do not cover the entire field of view. Using the SLM, the illumination pattern can be moved randomly, but eventually covering the entire field of view and imaging the scene iteratively.

Clearly, the non-orthogonal nature of the 6-needle pattern sets has significantly degraded the reconstructed image when using the TGI algorithm. By comparison, we note that the resolution of the reconstructed image achieved by a combination of OGI algorithm and distributed point spread functions is comparable (at the end of equal number of iterations; the equal number of iterations accounts for same dose for point scanning, TGI, and OGI in the optical context). Quantitatively, the spatial frequency and resolution is assessed using a radial contrast function (Fig. 4). The radial contrast is measured by unwrapping the reconstructed image iteratively from the center, with an increasing radius. The Fourier transform of this function gives a quantitative measurement of spatial frequency for targets such as the Siemens star, which have high spatial frequencies when approaching the center.

At the end of equal number of iterations, TGI has essentially converged to its final resolution, and any further improvements would primarily result in suppression of noise. OGI, on the other hand, has not yet converged but already significantly outperforms TGI for the non-orthogonal pattern set. Although the overall optical energy used in the 6-needle OGI and the traditional raster scan is the same, the peak flux in 6-needle approach is lower because of the distributed point spread function. This reduction is significant in situations where the sample can be damaged by high flux illumination, especially if that damage mechanism was nonlinear with respect to intensity. These mechanisms of equal dose but lesser damage at lower flux were shown in domains such as crystallography [54]. Subsequently, this verification of the pattern set and the OGI algorithm robustness sets the tone for application in TEM.

Computational ghost imaging in TEM

Building on the outcomes of the optical analogous experiment, we designed an experimental setup for applying computational OGI to TEM. Figure 5 shows a schematic representing the key

Downloaded from https://spj.science.org on April 24, 2023

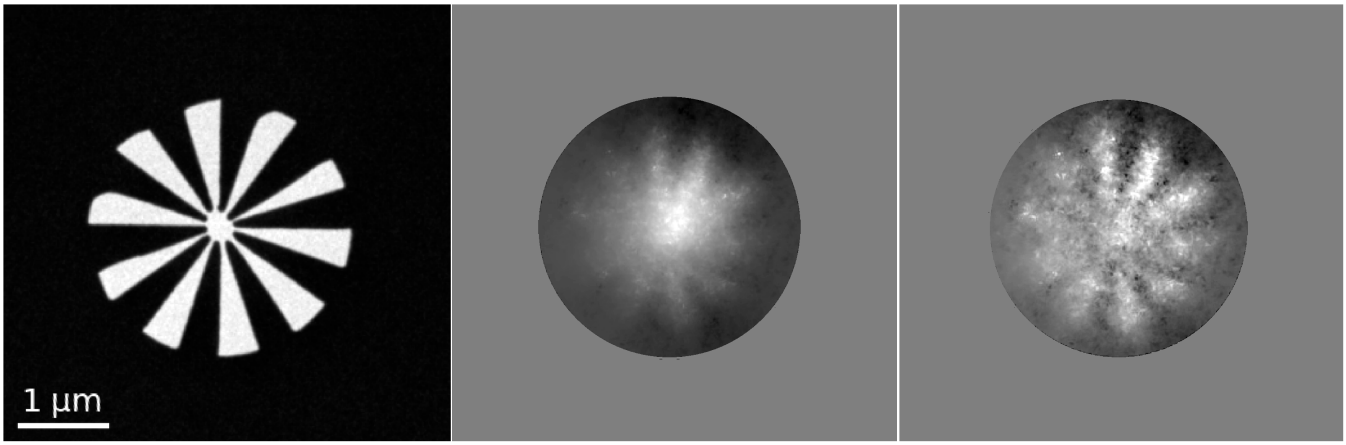

Fig. 6. The transmission electron microscope measures the intensity after the structured beam has interacted with the binary star target. For perspective, an image of the object (left) acquired using a Gatan MSC794 charge-coupled device camera is shown alongside image reconstructions using the TGI (middle) and OGI (right). The results clearly show a greater degree of resolution using structured beams and the OGI reconstruction algorithm.

steps of the experiment. To reproduce the structured illumination, we developed a custom Python algorithm that employs Fresnel integrals to simulate the free space propagation of electron beams. The simulations were carried out on a conventional desktop PC equipped with an Intel Core i7-8700 CPU and 32 GB of memory. Similar to the optical system, ghost imaging requires a reliable method for creating structured illumination. To solve this challenge, we developed a device (Fig. 5) that uses 6 electrically biased needles and applies a position-dependent phase shift to the beam. The beam shaping device produces complex patterns in the far field. The resulting point spread functions in the far field of the electron microscope are highly non-orthogonal. Therefore, we apply the proposed and optically verified OGI algorithm for imaging in the TEM setup.

The experiments were run on an FEI Tecnai F20 scanning transmission electron microscope. A MEMS-based electrostatic phase plate was inserted in the sample plane using a Thermo Fisher Scientific NanoEx-i/v sample holder. The imaged object of interest was inserted into the Selected Area aperture plane. In our experiments, we used the annular dark-field (ADF) detector as a bucket detector to collect the transmitted electrons and measure the intensity. To use the ADF detector, it has been necessary to use the microscope in STEM mode. We also developed a custom LabView interface for the simultaneous control of a multichannel power supply used to operate the MEMS-based electrostatic phase plate and a Keithley 2400 source meter used to measure the intensity registered by the ADF detector. The multichannel power supply features a Texas Instruments DAC81416 (digital to analog converter) and was operated between 2.5 and −2.5 V.

Having proven the applicability of computational OGI with the optical analogy, we demonstrate imaging with electron beams using the TEM system described (and shown in Fig. 5). The experiments were carried out with the modulation device (Fig. 2) placed in the path of the electron beam, between the electron gun and the object. The object, a multi-spoke star, is placed in the Selected Area plane of the microscope. It was fabricated on a commercially available 200-nm-thick Si_3N_4 membrane, covered with ∼150 nm of gold that acts as an amplitude mask. The transmitted energy is collected by the ADF detector, set off-axis to acquire the whole transmission. The output value of the detector is synchronised with the biases from the modulation device to maintain correlation of phase masks and corresponding detector measurements.

As mentioned previously, the structured illumination is reproduced using a Python algorithm, wherein the illumination pattern is predicted from the biases applied to the needles. The image reconstruction was done using 11,500 illumination patterns. Figure 6 shows the (left) target and the reconstruction results of the (middle) TGI and (right) OGI algorithms. Of these, the OGI algorithm (Eq. 3) clearly outperforms the TGI reconstruction. Qualitatively, the OGI algorithm produces a higher-resolution image reconstruction with better contrast in comparison to TGI techniques. For a more quantitative evaluation, we measured the peak signal-to-noise ratio (PSNR) for both reconstruction algorithms, obtaining values of 9.47 and 9.24 dB for the OGI and TGI, respectively. Even though the reconstruction is far from perfect, these preliminary results confirm a better performance for the new OGI methods. The image shows some imperfection in the left side of the reconstruction. Whereas the caustics have been accurately calibrated (see Appendix S2), residual microscope aberrations, inherent of this unconventional sample position, could locally reduce the quality of the reconstruction. Future investigation will require fast diagnostic of the aberrations as additional tool [55]. More in general, the results highlight the value, and the need for further investigation, of structured electron beams for imaging. While the optical data show clearly that OGI can match raster scanning (Fig. 4), higher resolutions with ghost imaging in TEM remain to be explored.

Conclusions

We have shown a successful ghost imaging algorithm that is robust to non-orthogonality of pattern sets and has proven its application in optical and electron microscopy regimes. In the optical regime, we combined non-orthogonal intensity distribution patterns with a novel ghost imaging algorithm for image reconstruction. The results show a comparable resolution between the proposed method and a point-scanning approach. In TEM, we showed a realization of phase modulation of the

Downloaded from https://spj.science.org on April 24, 2023

electron beam using charged needles. This phase modulation results in non-orthogonal illumination. Image reconstruction was achieved from these distributed point spread functions using the optically proven OGI algorithm with a reduced overall intensity illuminating the sample/object.

Acknowledgments

Funding: We wish to acknowledge support from the European Union's Horizon 2020 Research and Innovation Programme (grant agreement no. 766970 Project "Q-Sort" and no. 964591 "SMART-electron"), the Royal Society EPSRC Research Council funding to QuantIC (EP/M01326X/1), and the National Natural Science Foundation of China (grant no. 61922011 and U21B2034).
Author contributions: The optical investigation, methodology, experimentation, visualization, research coordination, communication, and original draft were prepared by A.K., with contributions from G.M.G. and M-J.S. (experimentation), and D.S. and R. Bowman (methodology). TEM contributions of methodology, investigation, and visualization and contributions to writing the draft were done by L.V. and E.R. Experimental contributions were made by P.R., S.F., R. Balboni, and A.M. V.G. was responsible for project administration, funding, conceptual discussions and contributions, project supervision, and review and editing of the manuscript for submission. M.J.P. contributed to the conceptualization, formal analysis, project supervision, and preparation of the manuscript. **Competing interests**: The authors declare that they have no competing interests.

Data Availability

The data generated and used to evaluate the conclusions of this paper can be made available upon reasonable request.

Supplementary Materials

Appendix S1. Dosage and damage when using an electron beam.
Appendix S2. Evaluation of the simulated electron patterns.

References

1. Chen Z, Jiang Y, Shao Y-T, Holtz ME, Odstrčil M, Guizar-Sicairos M, Hanke I, Ganschow S, Schlom DG, Muller DA. Electron ptychography achieves atomic-resolution limits set by lattice vibrations. *Science*. 2021;372(6544):826–831.
2. Verbeeck J, Béché A, Müller-Caspary K, Guzzinati G, Luong MA, Den Hertog M. Demonstration of a 2x2 programmable phase plate for electrons. *Ultramicroscopy*. 2018;190:58–65.
3. Li S, Cropp F, Kabra K, Lane TJ, Wetzstein G, Musumeci P, Ratner D. Electron ghost imaging. *Phys Rev Lett*. 2018;121(11):114801.
4. Egerton RF. Radiation damage to organic and inorganic specimens in the tem. *Micron*. 2019;119:72–87.
5. Konečná A, Rotunno E, Grillo V, de Abajo F, Vanacore GM. Single-pixel imaging in space and time with optically-modulated free electrons. arXiv. 2022. https://doi.org/10.48550/arXiv.2203.07332
6. Uchida M, Tonomura A. Generation of electron beams carrying orbital angular momentum. *Nature*. 2010;464(7289):737–739.
7. Verbeeck J, Tian H, Schattschneider P. Production and application of electron vortex beams. *Nature*. 2010;467(7313):301–304.
8. McMorran BJ, Agrawal A, Anderson IM, Herzing AA, Lezec HJ, McClelland JJ, Unguris J. Electron vortex beams with high quanta of orbital angular momentum. *Science*. 2011;331(6014):192–195.
9. Goutsoulas M, Efremidis NK. Dynamics of self-accelerating electron beams in a homogeneous magnetic field. *Phys Rev A*. 2021;103(1):Article 013519.
10. Voloch-Bloch N, Lereah Y, Lilach Y, Gover A, Arie A. Generation of electron Airy beams. *Nature*. 2013;494(7437):331–335.
11. Grillo V, Karimi E, Gazzadi GC, Frabboni S, Dennis MR, Boyd RW. Generation of nondiffracting electron bessel beams. *Phys Rev X*. 2014;4(1):Article 011013.
12. Grillo V, Harris J, Gazzadi GC, Balboni R, Mafakheri E, Dennis MR, Frabboni S, Boyd RW, Karimi E. Generation and application of bessel beams in electron microscopy. *Ultramicroscopy*. 2016;166:48–60.
13. Grillo V, Tavabi AH, Venturi F, Larocque H, Balboni R, Gazzadi GC, Frabboni S, Lu P-H, Mafakheri E, Bouchard F, et al. Measuring the orbital angular momentum spectrum of an electron beam. *Nat Commun*. 2017;8:Article 15536.
14. Tavabi AH, Rosi P, Rotunno E, Roncaglia A, Belsito L, Frabboni S, Pozzi G, Gazzadi GC, Lu P-H, Nijland R, et al. Experimental demonstration of an electrostatic orbital angular momentum sorter for electron beams. *Phys Rev Lett*. 2021;126(9):Article 094802.
15. Shiloh R, Lereah Y, Lilach Y, Arie A. Sculpturing the electron wave function using nanoscale phase masks. *Ultramicroscopy*. 2014;144:26–31.
16. Okamoto H, Latychevskaia T, Fink H-W. A quantum mechanical scheme to reduce radiation damage in electron microscopy. *Appl Phys Lett*. 2006;88:164103.
17. Shwartz S. Single-pixel imaging with high-energy electromagnetic radiation and particles. *Sci Bull*. 2021;66(9):857–859.
18. Rosi P, Venturi F, Medici G, Menozzi C, Gazzadi GC, Rotunno E, Frabboni S, Balboni R, Rezaee M, Tavabi AH, et al. Theoretical and practical aspects of the design and production of synthetic holograms for transmission electron microscopy. *J Appl Phys*. 2022;131:Article 031101.
19. Ruffato G, Rotunno E, Giberti L, Grillo V. Arbitrary conformal transformations of wave functions. *Phys Rev Appl*. 2021;15(5):Article 054028.
20. Griffiths DJ, Li Y. Charge density on a conducting needle. *Am J Phys*. 1996;64:706–714.
21. Matteucci G, Missiroli G, Muccini M, Pozzi G. Electron holography in the study of the electrostatic fields: The case of charged microtips. *Ultramicroscopy*. 1992;45(1):77–83.
22. Beleggia M, Kasama T, Larson DJ, Kelly TF, Dunin-Borkowski RE, Pozzi G. Towards quantitative off-axis electron holographic mapping of the electric field around the tip of a sharp biased metallic needle. *J Appl Phys*. 2014;116(2):Article 024305.
23. McMorran BJ, Harvey TR, Lavery MPJ. Efficient sorting of free electron orbital angular momentum. *New J Phys*. 2017;19:Article 023053.
24. Pozzi G, Grillo V, Lu P-H, Tavabi AH, Karimi E, Dunin-Borkowski RE. Design of electrostatic phase elements for sorting the orbital angular momentum of electrons. *Ultramicroscopy*. 2020;208:112861.
25. Tavabi AH, Migunov V, Dwyer C, Dunin-Borkowski RE, Pozzi G. Tunable caustic phenomena in electron wavefields. *Ultramicroscopy*. 2015;157:57–64.

Downloaded from https://spj.science.org on April 24, 2023

26. Sen P, Chen B, Garg G, Marschner SR, Horowitz M, Levoy M, Lensch HPA, Dual photography. *ACM Trans Graph*. 2005;24(3):745–755.
27. Duarte MF, Davenport MA, Takhar D, Laska JN, Sun T, Kelly KF, Baraniuk RG. Single-pixel imaging via compressive sampling. *IEEE Signal Process Mag*. 2008;25(2):83–91.
28. Kallepalli A, Innes J, Padgett MJ. Compressed sensing in the far-field of the spatial light modulator in high noise conditions. *Sci Rep*. 2021;11(1):17460.
29. Chen G, Wen ZQ, Qiu CW. Superoscillation: From physics to optical applications. *Light Sci Appl*. 2019;8:56.
30. Kallepalli A, Stellinga D, Sun M-J, Bowman R, Rotunno E, Grillo V, Padgett M, Ghost imaging with electron microscopy inspired, non-orthogonal phase masks. Research Square. 2021. https://doi.org/10.21203/rs.3.rs-1111193/v1
31. Wakin MB, Laska JN, Duarte MF, Baron D, Sarvotham S, Takhar D, Kelly KF, Baraniuk RG. An architecture for compressive imaging. Paper presented at: IEEE 2006. 2006 International Conference on Image Processing; 2006 Oct 8–11; Atlanta, GA, USA.
32. Candes EJ, Wakin MB. An introduction to compressive sampling. *IEEE Signal Process Mag*. 2008;25(2):21–30.
33. Romberg J. Imaging via compressive sampling. *IEEE Signal Process Mag*. 2008;25(2):14–20.
34. Jones L, Varambhia A, Beanland R, Kepaptsoglou D, Griffiths I,Ishizuka A, Azough F, Freer R, Ishizuka K, Cherns D, et al. Managing dose-, damage- and data-rates in multi-frame spectrum-imaging. *Microscopy*. 2018;67(1 Suppl):i98–i113.
35. Stantchev RI, Sun B, Hornett SM, Hobson PA, Gibson GM, Padgett MJ, Hendry E. Noninvasive, near-field terahertz imaging of hidden objects using a single-pixel detector. *Sci Adv*. 2016;2(6):Article e1600190.
36. Sun M-J, Zhang J-M. Single-pixel imaging and its application in three-dimensional reconstruction: A brief review. *Sensors*. 2019;19(3):732.
37. Howland GA, Dixon PB, Howell JC. Photon-counting compressive sensing laser radar for 3D imaging. *Appl Opt*. 2011;50(31):5917–5920.
38. Futia G, Schlup P, Winters DG, Bartels RA. Spatially-chirped modulation imaging of absorbtion and fluorescent objects on single-element optical detector. *Opt Express*. 2011;19(2):1626–1640.
39. Ferri F, Magatti D, Lugiato LA, Gatti A. Differential ghost imaging. *Phys Rev Lett*. 2010;104(25):253603.
40. Gibson GM, Johnson SD, Padgett MJ. Single-pixel imaging 12 years on: A review. *Opt Express*. 2020;28(19):28190–28208.
41. Shapiro JH. Computational ghost imaging. *Phys Rev A*. 2008;78(6):Article 061802.
42. Karp RM. Paper presented at: Proceedings of the IFIP 12th World Computer Congress on Algorithms, Software, Architecture - Information Processing '92, Volume 1 - Volume I; 1992. p. 416–429.
43. Gatti A, Brambilla E, Bache M, Lugiato LA. Ghost imaging with thermal light: Comparing entanglement and classical correlation. *Phys Rev Lett*. 2004;93(9):Article 093602.
44. Sun B, Welsh SS, Edgar MP, Shapiro JH, Padgett MJ. Normalized ghost imaging. *Opt Express*. 2012;20(15):16892–16901.
45. Pratt W, Kane J, Andrews H. Hadamard transform image coding. *Proc IEEE*. 1969;57(1):58–68.
46. Sloane NJA, Harwit M. Masks for hadamard transform optics, and weighing designs. *Appl Opt*. 1976;15(1):107–114.
47. Zhang Z, Wang X, Zheng G, Zhong J. Hadamard single-pixel imaging versus fourier single-pixel imaging. *Opt Express*. 2017;25(16):19619–19639.
48. Popa C, Zdunek R. Kaczmarz extended algorithm for tomographic image reconstruction from limited-data. *Math Comput Simul*. 2004;65(6):579–598.
49. Bautu A, Bautu E, Popa C. A weighted kaczmarz algorithm in image reconstruction. Proceedings of the Fifth Workshop on Mathematical Modelling of Environmental and Life Sciences Problems; 2006 Sep; Constanța, Romania.
50. Strohmer T, Vershynin R. A randomized kaczmarz algorithm with exponential convergence. *J Fourier Anal Appl*. 2008;15:262–278.
51. Pires RG, Pereira DR, Pereira LA, Mansano AF, Papa JP. Projections onto convex sets parameter estimation through harmony search and its application for image restoration. *Nat Comput*. 2016;15:493–502.
52. Sun M-L, Gu C-Q, Tang P-F. On randomized sampling kaczmarz method with application in compressed sensing. *Math Probl Eng*. 2020;2020:Article 7464212.
53. Boyd S, Parikh N, Chu E, Peleato B, Eckstein J. Distributed optimization and statistical learning via the alternating direction method of multipliers. *Found Trends Mach Learn*. 2011;3:1–122.
54. Karuppasamy M, Nejadasl FK, Vulovic M, Koster AJ, Ravelli RB. Radiation damage in single-particle cryo-electron microscopy: effects of dose and dose rate. *J Synchrotron Radiat*. 2011;18:(Pt 3)398–412.
55. Bertoni G, Rotunno E, Marsmans D, Tiemeijer P, Tavabi AH, Dunin-Borkowski RE, Grillo V, Near-real-time diagnosis of electron optical phase aberrations in scanning transmission electron microscopy using an artificial neural network. arXiv. 2022. https://doi.org/10.48550/arXiv.2204.11126

Downloaded from https://spj.science.org on April 24, 2023